Hole–hole Tamm–Dancoff-approximated density functional theory: A highly efficient electronic structure method incorporating dynamic and static correlation

Cite as: J. Chem. Phys. 153, 024110 (2020); doi: 10.1063/5.0003985
Submitted: 6 February 2020 • Accepted: 16 June 2020 •
Published Online: 9 July 2020

Christoph Bannwarth,[1,2] Jimmy K. Yu,[1,2,3] Edward G. Hohenstein,[1,2] and Todd J. Martínez[1,2,a)]

AFFILIATIONS

[1] Department of Chemistry and The PULSE Institute, Stanford University, Stanford, California 94305, USA
[2] SLAC National Accelerator Laboratory, 2575 Sand Hill Road, Menlo Park, California 94025, USA
[3] Biophysics Program, Stanford University, Stanford, California 94305, USA

[a)] **Author to whom correspondence should be addressed:** toddjmartinez@gmail.com

ABSTRACT

The study of photochemical reaction dynamics requires accurate as well as computationally efficient electronic structure methods for the ground and excited states. While time-dependent density functional theory (TDDFT) is not able to capture static correlation, complete active space self-consistent field methods neglect much of the dynamic correlation. Hence, inexpensive methods that encompass both static and dynamic electron correlation effects are of high interest. Here, we revisit hole–hole Tamm–Dancoff approximated (*hh*-TDA) density functional theory for this purpose. The *hh*-TDA method is the hole–hole counterpart to the more established particle–particle TDA (*pp*-TDA) method, both of which are derived from the particle–particle random phase approximation (*pp*-RPA). In *hh*-TDA, the *N*-electron electronic states are obtained through double annihilations starting from a doubly anionic (*N*+2 electron) reference state. In this way, *hh*-TDA treats ground and excited states on equal footing, thus allowing for conical intersections to be correctly described. The treatment of dynamic correlation is introduced through the use of commonly employed density functional approximations to the exchange-correlation potential. We show that *hh*-TDA is a promising candidate to efficiently treat the photochemistry of organic and biochemical systems that involve several low-lying excited states—particularly those with both low-lying $\pi\pi^*$ and $n\pi^*$ states where inclusion of dynamic correlation is essential to describe the relative energetics. In contrast to the existing literature on *pp*-TDA and *pp*-RPA, we employ a functional-dependent choice for the response kernel in *pp*- and *hh*-TDA, which closely resembles the response kernels occurring in linear response and collinear spin-flip TDDFT.

I. INTRODUCTION

Linear response time-dependent density functional theory (TDDFT) is the most commonly used electronic structure method for excited states due to its low computational cost and relative accuracy for absorption spectra involving valence excited states.[1] Unfortunately, due to the difficulties that presently available approximate exchange-correlation (XC) functionals encounter with near-degeneracies and static correlation, it is unsuitable for photochemical problems involving a conical intersection between the ground and first excited states.[2] While complete active space self-consistent field (CASSCF) methods can treat static electron correlation, they struggle to describe dynamic correlation.[3] Adding a correction to recover dynamic correlation (as in multireference perturbation theory[4] or multireference configuration interaction[5]) significantly increases the computational cost of the method and renders nonadiabatic dynamics simulations computationally intractable for many interesting medium to large sized molecules (although such dynamics is feasible for small molecules[6–12]).

There has long been interest in the development of inexpensive excited-state methods that can simultaneously treat dynamic and static correlation. One approach to this problem is to augment traditional multiconfigurational methods with semiempirical parameters. These parameters can be as simple as a constant scaling parameter applied to the energy[13] or as complex as a full semiempirical treatment of the Hamiltonian matrix elements.[14,15] While often successful, these methods may require cumbersome system-specific parameterization.[15–17] Alternatively, conventional multiconfigurational wavefunctions can be combined with a Kohn–Sham (KS) density functional theory (DFT)-based treatment of dynamic electron correlation.[18,19] Many of these methods use conventional multiconfigurational wavefunctions to capture static correlation and include a DFT-based treatment of dynamic correlation. Methods of this type include range-separated wavefunction/DFT methods,[20,21] multiconfigurational pair-density functional theory[22,23] (MC-PDFT), and combinations of DFT and configuration interaction,[24,25] such as in DFT/MRCI.[26,27] Alternative approaches attempt to incorporate multireference character directly in the DFT formalism by using an unconventional reference[28] or appealing to ensemble densities. Spin-flip TDDFT (SF-TDDFT)[29] is an example of a scheme based on an unconventional reference. Spin contamination problems have plagued DFT-based spin–flip methods;[30,31] however, this has recently been addressed by combining SF-TDDFT with *ad hoc* corrections from DFT/MRCI.[32] Ensemble formulations of DFT include the spin-restricted ensemble-referenced Kohn–Sham (REKS) methods.[33] To date, REKS methods need to be formulated specifically for the chosen ensemble (defined by an active space, as in CASSCF), and a general formulation applicable to arbitrary active spaces is lacking. Current implementations including gradients and nonadiabatic couplings are only applicable to an active space of two electrons in two orbitals.[34,35]

The recent development of particle–particle random phase approximation (*pp*-RPA) methods has opened new possibilities for inexpensive excited-state methods. The original aim of *pp*-RPA was to provide ground state correlation energies via an adiabatic connection fluctuation dissipation theorem (ACFDT) approach.[36–41] While the particle–hole RPA (*ph*-RPA) ACFDT approach recovers the ring channel of the correlation energy from the coupled cluster doubles (CCD) equations,[42] the ladder channel of the CCD correlation energy is obtained from the *pp*-RPA ACFDT approach.[36,41] Yang and co-workers also highlighted *pp*-RPA and its Tamm–Dancoff approximated *pp*-TDA variant as effective methods to compute electronic ground and excited state energies.[43–52] Starting from a doubly cationic ($N-2$)-electron reference, the N-electron ground state and excited states generated by excitations from the highest occupied molecular orbital (HOMO) are recovered by performing two-electron attachments.[45,49,50] This allows the treatment of the N-electron ground and excited states on equal footing (derived as simultaneous eigenvalues of a common Hamiltonian) at a computational cost comparable to the simplest excited state methods, e.g., TDDFT/*ph*-RPA and configuration interaction singles (CIS). Because the ground and excited states are treated on equal footing, *pp*-TDA based on an ($N-2$)-electron reference is able to predict the correct topography around conical intersections, as has been shown explicitly for H_3 and NH_3.[53] This is a major advance over conventional *ph*-TDDFT and CIS methods, which cannot reproduce conical intersections involving the ground state.[2]

In 2014, Peng *et al.* derived the *pp*-RPA equations from linear response theory by choosing a pairing field perturbation (termed TDDFT-P, see below in Sec. II A).[54] This formally allowed for the combination of *pp*-RPA and DFT references. Hence, the effect of dynamic correlation on the orbitals is incorporated through the exchange-correlation (XC) potential, while the *pp*-RPA and *pp*-TDA schemes ensure that ground and excited states are treated on equal footing and therefore can treat exact degeneracies correctly (see also Sec. II D).

In a procedure complementary to *pp*-TDA and *pp*-RPA based on an ($N-2$)-electron reference, the N-electron ground state and excited states can also be generated through double annihilations from a double anionic ($N+2$)-electron reference in which the lowest unoccupied molecular orbital (LUMO) is populated with two additional electrons. This ($N+2$)-electron *pp*-RPA scheme and its corresponding hole–hole (*hh*) Tamm–Dancoff approximation (*hh*-TDA) were first presented by Yang and co-workers.[49] Although the *pp*-RPA and *pp*-TDA methods based on an ($N-2$)-electron reference have now become quite established,[43–53] less attention has been paid to the hh-TDA method based on an ($N+2$)-electron reference. Yang and co-workers applied the *hh*-TDA method to oxygen and sulfur atoms[49] (noting "relatively large errors" in the results), but we have found no published reports of further developments or applications of *hh*-TDA to molecules. In this paper, we suggest that the *hh*-TDA method is worthy of renewed attention. Similar to the *pp*-TDA method, *hh*-TDA can effectively capture dynamic and static correlation in ground and low-lying excited states, including near- and exact degeneracies. Furthermore, the active orbital space in the ($N+2$)-electron-based *hh*-TDA appears to be suitable for the description of excited states in many organic molecules that are inaccessible to ($N-2$)-electron *pp*-TDA. Examples include molecules with low-lying $n\pi^*$ and $\pi\pi^*$ excited states that cannot be simultaneously described within *pp*-TDA (which, by construction, can only describe excited states where an electron is excited from the HOMO).

In contrast to previous work on *pp*-RPA, for both *pp*- and *hh*-TDA, we formulate the response kernel in a functional-specific way that resembles the kernels occurring in linear density matrix response theory. This new formulation of the response kernel is compared to the previously used functional-independent variant. We put particular emphasis on the utility of the *hh*-TDA method in the treatment of organic and biologically relevant systems involving both $\pi\pi^*$ and $n\pi^*$ transitions.

II. THEORY

A. Particle–particle random-phase approximation from pairing field perturbations

The particle–particle random phase approximation (*pp*-RPA) equations were derived by Peng and co-workers[54] by means of coupled time-dependent perturbation theory in analogy to well-established linear response theory by choosing a pairing field perturbation within the framework of Hartree–Fock (HF)/Kohn–Sham–Bogoliubov theory (termed TDDFT-P).[55] The ground state for this non-interacting particle system is defined by the zero-temperature grand potential as[54–57]

$$\Omega[\gamma,\kappa] = T_s[\gamma,\kappa] + V_{\text{ext}}[\gamma] + D_{\text{ext}}[\kappa] + E_{\text{JXC}}[\gamma,\kappa] - \mu N. \quad (1)$$

Here, $T_s[\gamma, \kappa]$ is the independent particle kinetic energy and $V_{\text{ext}}[\gamma]$ is the external potential energy, which contains the nuclear-electron attraction. $D_{\text{ext}}[\kappa]$ denotes the external pairing potential, and the last term preserves the total electron number. $E_{\text{JXC}}[\gamma, \kappa]$ is the mean-field potential energy due to the electrons and includes the particle–hole and particle–particle channels via the one-particle density matrix γ and the pairing matrix κ, respectively. The indices J, X, and C denote the Coulomb, exchange, and correlation components of this functional, respectively. The one-particle density matrix in the canonical molecular spin orbital basis is given by

$$\gamma_{pq} = \langle\Psi|a_p^\dagger a_q|\Psi\rangle = \delta_{pq}, \forall p,q \in \{\uparrow,\downarrow\}, \quad (2)$$

while the pairing matrix (or anomalous density matrix) is defined as

$$\kappa_{pq} = \langle\Psi|a_p a_q|\Psi\rangle, \kappa_{pq}^* = \langle\Psi|a_p^\dagger a_q^\dagger|\Psi\rangle, \forall p \in \{\uparrow\} \text{ and } q \in \{\downarrow\}. \quad (3)$$

Ψ refers to the single-determinant ground state wavefunction of the non-interacting Kohn–Sham (KS) system. Here and in the following, *i*, *j*, *k*, *l* denote occupied, *a*, *b*, *c*, *d* denote unoccupied, and *p*, *q*, *r*, *s* denote general molecular orbitals.

For the hypothetical true functional $E_{\text{JXC}}[\gamma, \kappa]$, the real-space density and anomalous density of the non-interacting KS system are identical to the respective quantities of the true interacting system. In the work of Peng *et al.*,[54] a non-superconducting system with no external pairing field in the ground state Hamiltonian is used. In that case, $D_{\text{ext}}[\kappa] = 0$. As a result, the mean-field potential energy is free from indirect electron–electron interactions (e.g., phonon-mediated interactions)[55] and contains only direct electron–electron interaction contributions via the (anti-symmetrized) Coulomb operator and XC potential. Based on the ground state defined by Eq. (1), Peng *et al.* derived the *pp*-RPA method by perturbing the ground state with an external pairing field. The TDDFT-P equations, which describe the coupled response to the pairing field perturbation, are given as[54]

$$-[\omega - (\varepsilon_i + \varepsilon_k - 2\mu)]\delta\kappa_{ik}(\omega) = \delta D_{ik}^{\text{ext}}(\omega) + \delta D_{ik}^{\text{JXC}}(\omega), \quad (4)$$

$$[\omega - (\varepsilon_a + \varepsilon_c - 2\mu)]\delta\kappa_{ac}(\omega) = \delta D_{ac}^{\text{ext}}(\omega) + \delta D_{ac}^{\text{JXC}}(\omega). \quad (5)$$

Here, $\delta\kappa_{pq}(\omega)$ are the first order changes in the pairing matrix induced by the external frequency-dependent pairing field perturbation $\delta D_{pq}^{\text{ext}}(\omega)$, ω is the frequency of the perturbation, ϵ_p is the orbital energy, and μ is the chemical potential or Fermi energy. The pairing matrix response $L_{pq,rs}$ of the mean field potential is contained in $\delta D_{pq}^{\text{JXC}}(\omega)$,

$$\delta D_{pq}^{\text{JXC}}(\omega) = -\sum_{j>l}^{N_{\text{occ}}} L_{pq,jl}\delta\kappa_{jl}(\omega) - \sum_{b>d}^{N_{\text{virt}}} L_{pq,bd}\delta\kappa_{bd}(\omega). \quad (6)$$

In our formulation of *pp*-RPA, the choice of $L_{pq,rs}$ differs from the one presented by Yang and co-workers,[44,45,54] as discussed in detail below.

B. The adiabatic particle–particle linear-response kernel

For a non-superconducting system in the absence of $D_{\text{ext}}[\kappa]$, the pairing matrix and its associated XC potential are zero in the electronic ground state. Consequently, only the γ-dependent terms in Eq. (1) survive, and minimizing the zero-temperature grand potential becomes equivalent to minimizing the standard KS or Hartree–Fock (HF) energy expression. It is only after taking the second derivatives with respect to κ that the particle–particle channels of the mean-field potential as in Eqs. (4) and (5) become non-zero. In the framework of *ab initio* wavefunction theory, the *pp*-RPA equations are based on a HF reference, and the mean-field potential takes the form of an anti-symmetrized Coulomb integral.[41] In that case, the *pp* and particle–hole (*ph*) channels of the mean-field potential are formally equivalent. We note, however, that only the exchange-type integral survives the spin integration in the *pp* channel (see the supplementary material).

In the context of approximate KS DFT, there may exist some liberty in choosing the explicit form of this response kernel. Given that contemporary semi-local density functional approximations (DFA) are defined for $\kappa = 0$, the pairing matrix response of the density functional drops out,

$$E_{\text{XC}}^{\text{DFA}}[\gamma,\kappa=0] = E_{\text{XC}}^{\text{DFA}}[\gamma] \rightarrow \frac{\partial^2 E_{\text{XC}}[\gamma]}{\partial\kappa_{pq}^*\partial\kappa_{rs}} = 0. \quad (7)$$

Yang and co-workers have already employed this approximation for the XC density functional response. Furthermore, they chose to use the HF-type mean-field response, i.e., a bare anti-symmetrized Coulomb integral, as the response kernel.[54] It is therefore independent of the underlying density functional approximation (DFA). With this kernel, the chosen DFA only affects the orbitals and orbital energies that enter the *pp*-RPA calculation, but not the *pp* response expression itself.

In this work, we employ a different choice for the *pp* response kernel. Given the formally equivalent *ph* and *pp* response kernels when using a HF reference,[41] which may be regarded as a special choice of the KS system, we draw analogy from the well-known *ph* linear response TDDFT. In spin-preserving[1,58] and spin–flip (SF)[29] formulations of TDDFT, the response kernel reflects the underlying ground state DFA in the way the non-local Fock exchange enters the response. Hence, we choose to use the same modification of the non-local Fock exchange, i.e., the global scaling and/or range-separation employed by the corresponding DFA,

$$L_{pq,rs} = [ps|qr] - a_X^{\text{FR}}[pr|qs] - a_X^{\text{SRA}}[pr|qs]^{\text{SRA}}. \quad (8)$$

The first term on the right-hand side corresponds to the Coulomb-type two-electron integral (Mulliken notation for spin MOs), whereas the remaining terms denote the modified exchange-type two-electron integrals. a_X^{FR} is the functional-specific scaling factor for the global [full-range (FR)] exchange integral,

$$[pr|qs] = \iint \phi_p^*(\mathbf{x}_1)\phi_r(\mathbf{x}_1)\frac{1}{r_{12}}\phi_q^*(\mathbf{x}_2)\phi_s(\mathbf{x}_2)\mathrm{d}\mathbf{x}_1\mathrm{d}\mathbf{x}_2. \quad (9)$$

Here, ϕ refers to a molecular spin orbital and $\mathbf{x}_1/\mathbf{x}_2$ denote all spatial and spin coordinates of electrons 1/2. The short range-attenuated

(SRA) part of the exchange integral employs the modified Coulomb operator and is given as

$$[pr|qs]^{\mathrm{SRA}} = \iint \phi_p^*(\mathbf{x}_1)\phi_r(\mathbf{x}_1)\frac{\mathrm{erf}(\omega_{\mathrm{SRA}} r_{12})}{r_{12}}\phi_q^*(\mathbf{x}_2)\phi_s(\mathbf{x}_2)\mathrm{d}\mathbf{x}_1\mathrm{d}\mathbf{x}_2. \tag{10}$$

Like Yang and co-workers, we also assume the pairing matrix response of the XC functional to be zero [see Eq. (7)], allowing the response kernel to become frequency independent. Due to spin integration (note the definition of the pairing matrix), the Coulomb part in the *pp* response kernel is zero; hence,

$$L_{p\bar{q},r\bar{s}} = -a_X^{\mathrm{FR}}(pr|\overline{qs}) - a_X^{\mathrm{SRA}}(pr|\overline{qs})^{\mathrm{SRA}}. \tag{11}$$

Here, we have used the Mulliken notation for spatial MOs and overbarred orbital indices to highlight orbitals corresponding to β spin. Our choice for the response kernel [Eq. (11)] is identical to the one in collinear SF-TDDFT but with inverted sign [note that $L_{pq,rs}$ is subtracted in Eq. (14) below]. This can be understood from a second quantization picture in which both the spin–flip and *pp*-RPA approaches apply creation/annihilation operators acting on different spin, i.e., $a_\uparrow^\dagger a_\downarrow$ in spin–flip and $a_\uparrow^\dagger a_\downarrow^\dagger / a_\uparrow a_\downarrow$ in the *pp*/*hh* channels. Therefore, only the exchange integral does not vanish upon spin integration, as in *pp*-RPA, and the flipped sign results from the commutation relation of the annihilation and creation operators (see the supplementary material for a comparison). SF-TDDFT can be derived from linear-response *ph* TD-DFT if changes in the density matrix that do not preserve the $\hat{S}_z$ expectation value are allowed.[29] Due to its origin from an analogy to linear response SF-TDDFT, we refer to our choice of the response kernel, Eq. (11), as the linear response-type kernel in the following to distinguish it from the DFA-independent, HF-like kernel used by Yang and co-workers.[49]

C. The hole–hole Tamm–Dancoff approximated pp-RPA method

Using the response kernel in Eq. (11), we can rewrite Eqs. (4) and (5) in matrix notation as

$$\left[\begin{pmatrix}\mathbf{A}^{pp} & \mathbf{B}^{ph}\\ \mathbf{B}^{hp} & \mathbf{A}^{hh}\end{pmatrix} - \begin{pmatrix}\omega & 0\\ 0 & -\omega\end{pmatrix}\right]\begin{pmatrix}\boldsymbol{\kappa}^{pp}(\omega)\\ \boldsymbol{\kappa}^{hh}(\omega)\end{pmatrix} = \begin{pmatrix}\delta\mathbf{D}^{pp}(\omega)\\ \delta\mathbf{D}^{hh}(\omega)\end{pmatrix}. \tag{12}$$

Here, the superscripts *pp* and *hh* define the particle–particle (double creation in the virtual space) and hole–hole (double annihilation in the occupied space) blocks, respectively. $\mathbf{A}^{pp}$ is of dimension $n_{\mathrm{virt}}^2 \times n_{\mathrm{virt}}^2$, and $\mathbf{A}^{hh}$ is of dimension $n_{\mathrm{occ}}^2 \times n_{\mathrm{occ}}^2$. Their elements are given as

$$[\mathbf{A}^{pp}]_{ac,bd} = A_{ac,bd} = \delta_{ab}\delta_{cd}(\epsilon_a + \epsilon_c - 2\mu) - L_{ac,bd} \tag{13}$$

and

$$[\mathbf{A}^{hh}]_{ik,jl} = A_{ik,jl} = -\delta_{ij}\delta_{kl}(\epsilon_i + \epsilon_k - 2\mu) - L_{ik,jl}. \tag{14}$$

$\mathbf{B}^{hp} = [\mathbf{B}^{ph}]^T$ is of dimension $n_{\mathrm{occ}}^2 \times n_{\mathrm{virt}}^2$ and is given as

$$B_{ik,bd} = -L_{ik,bd}. \tag{15}$$

If we now let the perturbation [right-hand side in Eq. (12)] go to zero, we find that there are non-trivial solutions to this system of equations, which correspond to the poles of the particle–particle/hole–hole response function. This leads to the non-Hermitian eigenvalue problem

$$\begin{pmatrix}\mathbf{A}^{pp} & \mathbf{B}^{ph}\\ \mathbf{B}^{hp} & \mathbf{A}^{hh}\end{pmatrix}\begin{pmatrix}\mathbf{X}\\ \mathbf{Y}\end{pmatrix} = \begin{pmatrix}\mathbf{X}\\ \mathbf{Y}\end{pmatrix}\begin{pmatrix}\boldsymbol{\omega} & 0\\ 0 & -\boldsymbol{\omega}\end{pmatrix}. \tag{16}$$

Employing the commonly used notation,[54] the matrices $\mathbf{X}$ and $\mathbf{Y}$ contain the eigenvectors, which correspond to the *pp* and *hh* changes in the pairing matrix κ. $\boldsymbol{\omega}$ is a diagonal matrix, which contains the eigenvalues of the non-Hermitian eigenvalue problem. If we neglect the coupling matrices $\mathbf{B}^{hp}$ and $\mathbf{B}^{ph}$ between the *pp* and *hh* blocks, we obtain the so-called Tamm–Dancoff approximated (TDA) eigenvalue problems,

$$\mathbf{A}^{pp}\mathbf{X} = \mathbf{X}\boldsymbol{\omega}^{pp} \tag{17}$$

for the *pp*-TDA case and

$$\mathbf{A}^{hh}\mathbf{Y} = \mathbf{Y}\boldsymbol{\omega}^{hh} \tag{18}$$

for the *hh*-TDA problem.

Note that within TDA, the constant diagonal shift of $\mp 2\mu$ in Eqs. (13) and (14) can be removed from the definition of the corresponding matrix elements. Both of these eigenvalue problems are guaranteed to have only real eigenvalues. This makes them more robust than the full *pp*-RPA case, which can have complex solutions that spoil the potential energy surfaces (PES) around conical intersections (as noted in the context of coupled cluster theory[59,60]). While the *pp*-TDA method based on an (N–2)-electron reference has been extensively investigated as a method to describe low-lying excited states[45,49] and S_0/S_1 conical intersections,[53] the *hh*-TDA method has been less thoroughly explored for the molecular electronic structure.[49] In this work, we suggest that *hh*-TDA should be revisited as an efficient DFT-based method capable of computing low-lying excited states even in the presence of conical intersections.

Before benchmarking the *hh*-TDA method along with our choice for the response kernel [Eq. (11)], we will briefly discuss some practical aspects of the *pp*-TDA and *hh*-TDA methods in Sec. II D.

D. Practical considerations of the *pp*-TDA and *hh*-TDA methods

In both the *pp*-TDA and *hh*-TDA methods, the N-electron target system is described by first solving the ground state electronic structure for a system that differs by two electrons from the N-electron target system. This corresponds to a double cation (N–2 electrons) in the case of *pp*-TDA or a double anion (N+2 electrons) in the case of *hh*-TDA. The ground and excited states of the N-electron target system are then obtained by creation (*pp*-TDA) or annihilation (*hh*-TDA) of two electrons (see Fig. 1).

The inability to describe either doubly excited states or conical intersections involving the ground state are well-known shortcomings of standard single-reference methods such as linear-response

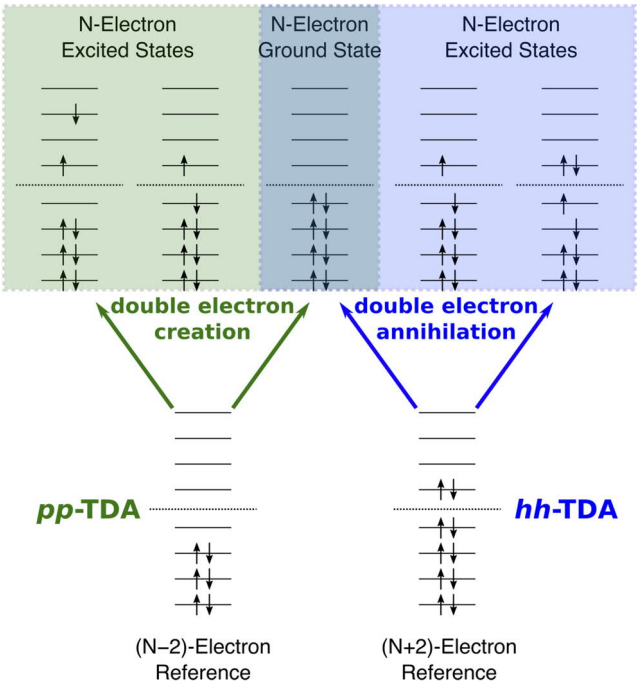

FIG. 1. Graphical representation of the *pp*-TDA (left) and *hh*-TDA (right) methods to obtain the *N*-electron ground state and excited states. In the *pp*-TDA case (left), the orbitals are obtained from a SCF calculation on the (*N*−2)-electron system. Addition (green) of two electrons into the virtual space recovers the *N*-electron ground and excited states. The closed-shell *N*-electron ground state obtained from *pp*-TDA is dominated by the configuration that corresponds to a double creation in the LUMO [with respect to the (*N*−2)-electron system]. In the *hh*-TDA case (right), the orbitals are obtained from a SCF calculation on the (*N*+2)-electron system. Annihilation (blue) of the two electrons in the occupied orbital space then recovers the *N*-electron ground and excited states. Here, the *N*-electron ground state is dominated by the configuration that corresponds to a double annihilation in the HOMO [with respect to the (*N*+2)-electron reference].

(*ph*) TD-DFT and CIS. These are both rectified by *pp*- and *hh*-TDA. Since the ground and the excited states are solutions of the same eigenvalue problem, near- and exact degeneracies (such as conical intersections) can be properly described. Furthermore, some doubly excited states can be computed (see Fig. 2). At the same time, the preceding ground state calculation of the double ionic state is of single-reference complexity and incorporates dynamic correlation by virtue of the XC potential. Therefore, both *pp*- and *hh*-TDA schemes are, in principle, able to capture static and dynamic correlation, making them promising methods for use in nonadiabatic dynamics simulations. Furthermore, in contrast to the SF-TDDFT scheme, pure eigenfunctions of $\hat{S}^2$ are obtained trivially in both *pp*- and *hh*-TDA.

However, both methods also have some obvious shortcomings in common. First, the excited state expansion space is highly restricted. Taking the *N*-electron target system as reference, *pp*-TDA only includes excitations *from* the HOMO, while *hh*-TDA is restricted to excitations *to* the LUMO. Second, both methods take a detour by computing the orbitals for a reference that differs in its total charge from the target state, as SF-TDDFT does with a differing spin state. As a result, two-state degeneracies of the *N*-electron state can be treated at the cost of a single reference method. However, the orbitals are not optimized for the *N*-electron system. This may have a significant implication for dynamics simulations: a degeneracy on the (*N*+2) or (*N*−2) surface itself can occur and cause instabilities in the SCF procedure.

Zhang *et al.* noted that the choice of a (*N*+2) reference may be hampered by the existence of unbound orbitals.[50] Presumably, this is one of the reasons that the *hh*-TDA method has not received serious attention in molecular electronic structure so far. There are two distinct consequences of unbound orbitals that can be envisioned. The first consequence is quite practical, namely, that it may be difficult to converge the SCF procedure for the (*N*+2) reference. In the usual *hh*-TDA method, non-convergence of the SCF procedure for the (*N*+2) reference would be fatal. The second consequence is somewhat more formal. Even if SCF convergence can be achieved, orbitals with positive orbital energies do not correspond to bound electrons. They can thus be very sensitive to the employed basis set. Indeed, with a sufficiently flexible basis set, they would be expected to be highly delocalized continuum functions and poor representatives of a low-lying valence excited state.

Regarding the first consideration, we note that poor convergence of the SCF procedure will be exacerbated if the long-range potential is incorrect. DFAs with 100% long-range Fock exchange are known to capture the asymptotic potential correctly. Accordingly, using DFAs with 100% long-range exchange, we have not observed any instability of the (*N*+2)-electron SCF procedure for the molecules we tested. Even the green fluorescent protein chromophore (HBI) anion with a net charge of −3 for the reference state converges without difficulty when an asymptotically correct, range-separated DFA is used. However, the *hh*-TDA method is likely to encounter serious SCF convergence difficulties for DFAs that do not incorporate long-range exact exchange.

It has been previously observed that finite-basis set DFT is capable of providing reasonable electron affinities computed as energy differences $\mathrm{EA} = E_{\mathrm{N}} - E_{\mathrm{N+1}}$, even when the anion has unbound occupied orbitals.[61] This suggests that the second consideration is largely formal. However, there are also some practical concerns. The success of *hh*-TDA in describing excited states is predicated on the HOMO orbital of the (*N*+2)-electron determinant being a good approximation to the bound orbital that predominantly contributes to the low-lying *N*-electron excited states. This will certainly not hold if the HOMO is a good approximation to a continuum orbital, which is the expected outcome in a sufficiently large basis set. We take a practical approach here and recommend that diffuse basis sets should be avoided in the context of *hh*-TDA. For the finite orbital basis sets of double- or triple-zeta quality used in this study, there are very few cases where the *hh*-TDA scheme based on an (*N*+2)-electron reference fails, in spite of the presence of occupied orbitals with positive energies. This implies that the HOMO of the (*N*+2)-electron system is a good approximation to the LUMO of the N-electron system, albeit with shifted orbital energies. This shift is effectively removed during the *hh*-TDA step, leading to a reasonable description of the relative energies between the *N*-electron ground and low-lying excited states. We will further elaborate on this issue in Sec. IV E, but we emphasize again that diffuse basis sets should

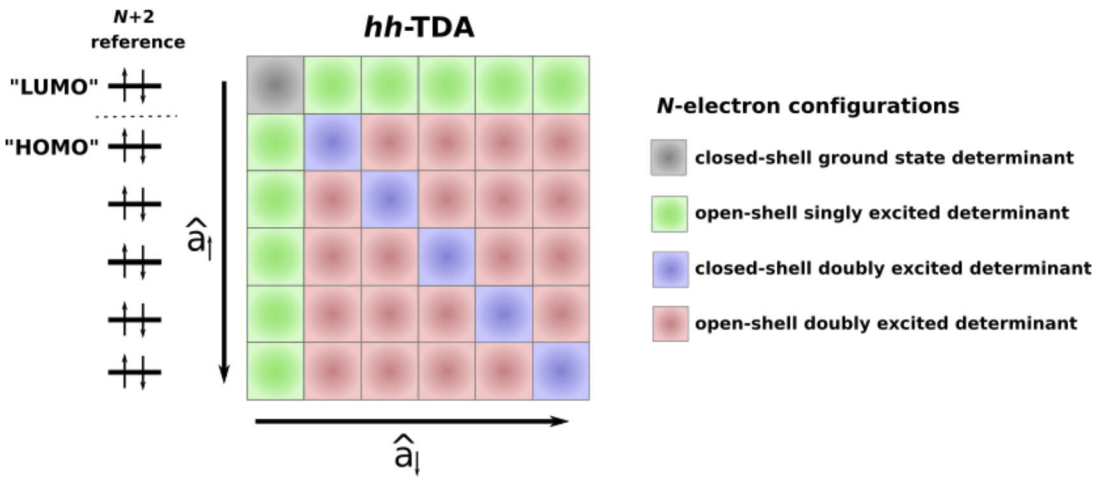

FIG. 2. Schematic representation of the excitation types generated in *hh*-TDA with respect to the *N*-electron ground state. The "LUMO" and "HOMO" orbitals are defined with respect to the *N*-electron ground state determinant.

usually be avoided in combination with the (*N*+2)-electron reference calculation.

For *pp*-TDA, there may also exist a practical implication with respect to the underlying DFA. It was shown that *pp*-RPA based on a HF reference leads to less accurate singlet-triplet splittings,[48] slower basis set convergence,[45] and overall less accurate excitation energies for small molecules[45] than *pp*-RPA based on DFAs with little or no exact exchange. Similar results for excitation energies were reported for *pp*-TDA.[45] A convenient test case is the $\pi\pi^*$ state of ethylene, where both *hh*-TDA and *pp*-TDA provide a suitable active orbital space. Accurate methods such as coupled cluster and multireference perturbation theory agree that this should be the lowest valence excited state. For ethylene, we observe a stronger dependence on the amount of Fock exchange in the DFA for *pp*-TDA (Table S13 in the supplementary material). The $\pi\pi^*$ state is the fourth excited state for *pp*-TDA-HF, while it is the second excited state for *hh*-TDA-HF. It is well-known that adding Fock exchange to a DFA increases the differential treatment of virtual and occupied orbitals. In molecular systems,[62] the virtual orbitals in HF are best suited to describe electron attachment, while virtual orbitals in (semi-)local DFT are more appropriate to describe electronic excitations.[63] This implies that DFAs with large amounts of exact exchange will raise the energy of the HOMO of the *N*-electron target system in *pp*-TDA. Therefore, when using practical DFAs, the optimal amount of exact exchange could be different for *pp*-TDA and *hh*-TDA, and this point deserves further study. In this work, we focus on DFAs for the linear-response-type kernel *hh*-TDA framework.

We will note (details in Table S13) that the ordering of the $\pi\pi^*$ state for ethylene in *pp*-TDA is improved by using our linear response-type kernel compared to the previously introduced functional-independent HF-type response kernel.[45,49,54] For clarity, it should be noted that purely (semi-)local DFAs have a vanishing response kernel in our linear-response-type formulation, i.e., $\mathbf{A}^{pp}$ and $\mathbf{A}^{hh}$ are diagonal in that case. In the HF-type response kernel, the bare anti-symmetrized Coulomb integral is used as the response kernel, regardless of the underlying DFA.

In *hh*-TDA, within the limitations of the given basis set (see above), the LUMO (with respect to the *N*-electron target system) is generated on equal footing with the occupied orbitals for HF or any DFA. Another difference between *hh*- and *pp*-TDA is the dimension of the $\mathbf{A}$ matrix to be diagonalized. In *pp*-TDA, this dimension increases strongly with the size of the atomic orbital (AO) basis. For *hh*-TDA, the dimensions are independent of the basis set size (unless effective core potentials are used).

We mention for the sake of completeness that *pp*-TDA-HF is equivalent to full configuration interaction (FCI) for any two-electron system, while *hh*-TDA-HF is equivalent to FCI for an *N*-electron system in a basis that provides exactly two virtual molecular spin orbitals. We have confirmed this via calculations on H_2 in an STO-3G basis set (see the supplementary material). Thus, both schemes have similarities to CASCI methods with a fixed active space (i.e., *N* electrons in $N/2 + 1$ orbitals for *hh*-TDA and two electrons in $n_{\text{virt}} + 1$ orbitals for *pp*-TDA). One can speculate that the ability of the *pp*-TDA and *hh*-TDA to describe static correlation arises from their similarity to CASCI methods. For the same reason, however, neither *pp*-TDA nor *hh*-TDA is size consistent. As long as no degeneracy of the LUMO/LUMO+1 (*hh*-TDA) or the HOMO/HOMO−1 (*pp*-TDA) is present, this is not expected to have practical implications for the description of relative energies between electronic states.

III. COMPUTATIONAL DETAILS

The *hh*-TDA and *pp*-TDA methods have been implemented in the electronic structure code TeraChem.[64,65] All *hh*-TDA and *pp*-TDA calculations in this work are performed with this development version of TeraChem. To compare with the *pp*-TDA data in the literature, we have implemented our choice for the response kernel [Eq. (11)] as well as the HF-type response kernel of Yang and

co-workers.[54] We confirmed that our implementation is correct by comparison of *pp*-TDA excitation energies with values reported in the literature[45] as well as comparisons between CASCI and *hh*/*pp*-TDA using Hartree–Fock reference states.

In the functional assessment for vertical excitation energies with *hh*-TDA in Sec. IV A, we considered the global hybrid functionals B3LYP,[66–69] PBE0,[70,71] and BHLYP[66,67,72] as well as Hartree–Fock. Thus, we cover different amounts of non-local Fock exchange in the mean field Hamiltonian (20%, 25%, 50%, and 100%, respectively). Additionally, we test different range-separated hybrid functionals, namely, CAM-B3LYP,[66–69,73] ωPBEh,[74] and the B97[75] type functionals: ωB97,[76] ωB97X,[76] and ωB97X-D3.[77] For clarity, it is emphasized that the latter two are different in their functional parameters (see the supplementary material) and hence should give rise to different electronic structures. The DFA assessment is restricted to the linear response-type kernel variant of *hh*-TDA [Eq. (11)] For the assessment of different functionals, we employed the spherical split-valence atomic orbital def2-SV(P)[78,79] basis set by Ahlrichs and co-workers. All SCF calculations used the converged Hartree–Fock orbitals as guess orbitals. The systems considered in this work are given in the supplementary material.

When comparing *pp*-TDA and *hh*-TDA in Sec. IV B, we use the same spherical TZVP basis set[80] that has been used in the original benchmark papers by Thiel and co-workers.[81] Both schemes are employed in a setting, in which the occupied and active orbitals have been generated on equal footing, i.e., where these orbitals experience a mean-field potential with the same number of electrons. The *pp*-TDA is hence combined with the generalized gradient approximation (GGA) functional PBE[70] (see also Sec. II D). *hh*-TDA is combined with the range-separated functional ωB97X,[76] which is shown to be a well-performing combination in Sec. IV A (and in the supplementary material). We consider both the linear response-type (this work) and the HF-type (Yang and co-workers) response kernels for *pp*-TDA and *hh*-TDA. Additionally, we have performed *ph* Tamm–Dancoff approximated TDDFT calculations with the ωB97X functional. For reference, we use the best estimates for excitation energies of Thiel and co-workers[81] and complement these with equation-of-motion singles and doubles coupled cluster (EOM-CCSD) calculations (the same basis set) as implemented in Q-Chem v5.0.0.[82]

In Sec. IV C 1, we calculate the ethylene potential energy surface (PES) with *hh*-TDA-ωB97X (linear response kernel) using the Cartesian def2-SVP[78,79] basis set. The scans along the pyramidalization and torsion angles were performed without relaxation of the remaining degrees of freedom.

The excited state energies of thymine at three critical structures are considered in Sec. IV C 2. We use *hh*-TDA in combination with the ωPBE functional and the Cartesian 6-31G** basis set.[83–85] A range separation parameter ω = 0.2 a.u. was selected after a coarse scan and comparison against high level reference values for this molecule. We calculated these reference values with EOM-CCSD/aug-cc-pVDZ with Q-Chem. While the Franck–Condon (FC), the S_1 minimum, and the S_1/S_2 minimum energy conical intersection (MECI) were optimized with *hh*-TDA, we used the respective coupled cluster (CC) geometries of Ref. 86 for single-points at the EOM-CCSD/aug-cc-pVDZ level of theory. The S_2 ($\pi\pi^*$) saddle point geometry therein is claimed to be "in close proximity" to the conical intersection seam.[86] Due to the lack of a properly CC-optimized MECI structure, we use that structure as a substitute and estimate the MECI energy by averaging the S_1 and S_2 energies computed with EOM-CCSD/aug-cc-pVDZ.

In Sec. IV C 3, we apply *hh*-TDA with the ωB97[76] functional in combination with the Cartesian 6-31G** basis set[83–85] and compare to results obtained with multireference configuration interaction methods including single and double excitations (MRSDCI).[87]

IV. RESULTS

A. Functional benchmarking for hh-TDA

The performance of density functionals for the calculation of vertical excitation energies in the linear-response *ph* time-dependent density functional theory framework is well known[88] and the role of Fock exchange is fairly well understood.[1] In contrast, for the *hh*-TDA method proposed in this work, the impact of Fock exchange and the use of an anionic reference on the excitation energies is not known. Therefore, we start by benchmarking several common DFAs along with Hartree–Fock (HF) in the calculation of vertical excitation energies with *hh*-TDA.

To gain more insight, we consider the lowest vertical excitation energies using molecules and reference data from previously published datasets where highly accurate excitation energies are available.[81,89,90] We classify the excitation type into different categories: intermolecular charge-transfer (CT) and predominantly local excitations. We also consider molecules that have push–pull type excitations, i.e., excitations with partial intramolecular CT character. We find that the functionals behave similarly for this set as for the local excitations. Thus, we have added them to the latter set and distinguish only intermolecular CT and intramolecular excitations (see the supplementary material for separate results of the local and the push–pull set). In the latter set, we have selected molecules for which *hh*-TDA, across different DFAs, produces the same character for the lowest vertical excitation as the reference method (SCS-CC2[91]).

We have not considered any purely semi-local GGA-type DFAs since these show severe convergence problems in the self-consistent field (SCF) procedure of the double anionic reference (see also Sec. II D). Although we also expect that global hybrids will not be optimal in that case, for completeness, we have included some prototypical global hybrid functionals that differ in the amount of Fock exchange. All functionals considered are listed in Sec. III, but we restrict the discussion in this paper to the globally constant Fock-exchange DFAs B3LYP, BHLYP, and HF (these functionals contain 20%, 50%, and 100% of Fock exchange, respectively). Furthermore, we find that all tested range-separated DFAs with 100% long-range exchange perform similarly; therefore, we restrict the current discussion to the ωB97X-D3 functional. The results for the other functionals that were tested can be found in the supplementary material.

Figure 3 shows the Gaussian error distributions based on the mean deviation (MD) and standard deviation (SD) obtained for the aforementioned reference datasets of excitation energies. While *hh*-TDA-HF yields CT excitation energies that are on average underestimated by almost 1 eV, the excitation energies for locally excited states show a systematic overestimation of about the same magnitude. Furthermore, the error is significantly more systematic for the

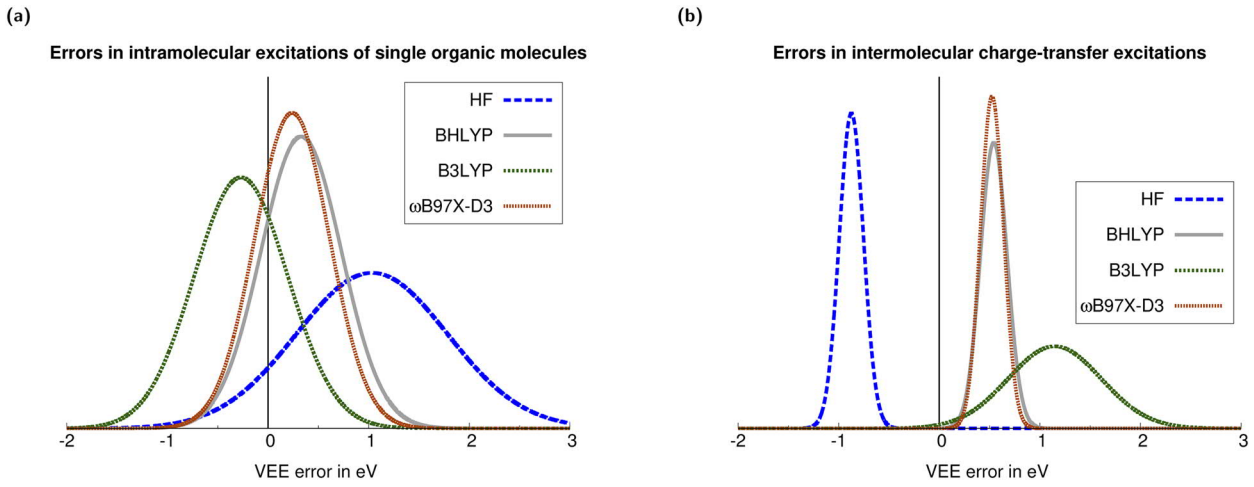

FIG. 3. Gaussian error distribution functions for *hh*-TDA with different density functional approximations in the calculation of vertical excitation energies (VEEs). The spherical def2-SV(P)[78,79] basis set and the LR kernel in the *hh*-TDA calculation have been used throughout. The centers of the Gaussians correspond to the mean deviation (MD), whereas the width of the Gaussian corresponds to the standard deviation (SD), both in eV. (a) Lowest vertical excitations of single molecules with no or little intramolecular CT character. The individual MDs and SDs in eV are B3LYP (−0.27, 0.47), BHLYP (0.33, 0.40), HF (1.03, 0.75), and ωB97X-D3 (0.24, 0.37), with N = 27. (b) Intermolecular CT excitations of organic bimolecular complexes. The individual MDs and SDs in eV are B3LYP (1.15, 0.46), BHLYP (0.54, 0.13), HF (−0.87, 0.12), and ωB97X-D3 (0.52, 0.11), with N = 6. See the supplementary material for details on the benchmark sets and results with other functionals.

intermolecular CT excitations. For DFAs with low amounts of Fock exchange, i.e., B3LYP, these trends are reversed, however, with a smaller magnitude for the underestimation of local excitation energies. It is noteworthy that the DFAs behave quite different than in a *ph* linear response TD-DFT framework. In the latter, DFAs with low amounts of Fock exchange significantly underestimate CT excitations.[89] The BHLYP functional, which is in between in terms of the percentage of Fock exchange, shows more consistent errors for both sets (MD ≈ 0.4 eV–0.5 eV), as well as more narrow error distributions. The range-separated DFA ωB97X-D3 behaves even slightly better than BHLYP. This, along with the fact that the 100% asymptotic Fock exchange makes these DFAs less prone to SCF convergence issues with the (N+2)-electron reference, suggests the use of asymptotically correct range-separated hybrid functionals in combination with the *hh*-TDA scheme.

In addition to benchmarking the DFAs for CT and local states, we investigate state splittings between ππ* and locally excited states with different character (mostly $n\pi^*$). For this purpose, we have selected a set of systems mostly comprised of molecules from Thiel's 2008 benchmark set.[81,90] Problematic systems, which are impossible to treat with *hh*-TDA due to the restricted orbital space, were discarded from the benchmark set. These are systems in which either the population of the frontier orbitals in the (N+2)-electron system is not clear (degenerate LUMOs in the N-electron determinant) or the excited states cannot predominantly be described by a single orbital–orbital transition (benzene, naphthalene, pyrrole, and *s*-triazine). Furthermore, butadiene, hexatriene, and octatetraene are not considered here but in Sec. IV B. The results are visualized in Fig. 4, while the respective symmetry labels and results for other density functionals can be found in the supplementary material. First, we stress the relevance of high amounts of Fock exchange in the DFA, which we mentioned earlier in Sec. II D. We find that B3LYP and BHLYP, but also a few range-separated functionals (CAM-B3LYP or ωPBEh, see supplementary material), show incorrect orbital occupations for some carbonyl systems in the (N+2)-electron SCF calculation, i.e., the HOMO of the (N+2)-electron system does not correspond to the LUMO obtained from

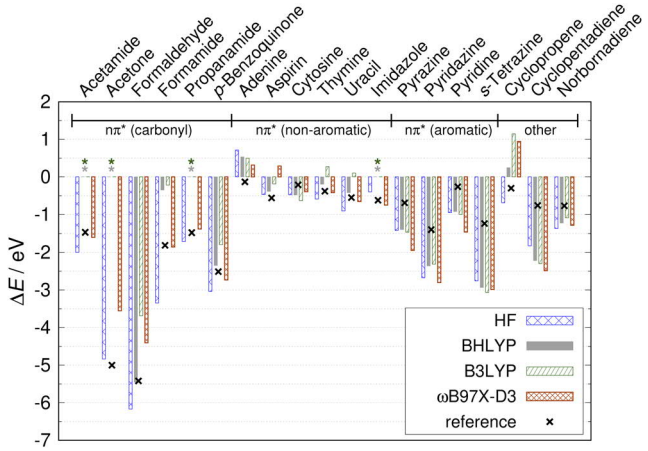

FIG. 4. Energetic splitting between a low-lying ππ* and another (usually $n\pi^*$) excited state. The excitation energies were computed at the *hh*-TDA level of theory (LR kernel) employing the spherical def2-SV(P) basis set. A π-system is classified as "aromatic," if a near-degeneracy of the N-electron system LUMO can be expected, due to the symmetry of the molecule (cf. Frost circle representation). An asterisk marks missing data due to an incorrect LUMO (with respect to the N-electron system) occupation in the (N+2)-electron SCF calculation. The reference values are taken from Ref. 81 (aspirin from Ref. 90). The respective state symmetries are given in the supplementary material.

an SCF calculation on the N-electron system. Hence, the excited states for these systems cannot be described properly with these functionals.

We also find that the global hybrid functionals perform poorly for the state splittings compared to Hartree–Fock or range-separated functionals (e.g., ωB97X-D3). Except in two cases ($n\pi^*/\pi\pi^*$ in aspirin and $\sigma\pi^*/\pi\pi^*$ in cyclopropane), the latter two perform similarly. Both describe the $n\pi^*$ splittings reasonably well, while systematically overestimated $\pi\pi^*$ excitations are found for aromatic systems, regardless of which DFA is used. This seems to be caused by the absence of accessible higher lying anti-bonding π orbitals in the expansion space, which would lower these excitations and improve the energetic splittings with respect to the $n\pi^*$ excitations. This is also observed for the splittings between the different $\pi\pi^*$ states in cyclopentadiene and norbornadiene, presumably for the same reasons. Interestingly, reduced short-range Fock exchange leads to increased $\sigma\pi^*$ excitation energies in cyclopropene, which then lead to qualitatively incorrect energy splittings with respect to the $\pi\pi^*$ state. This is observed for all DFAs, and only HF ranks these states qualitatively correctly.

Overall, the results indicate that the *hh*-TDA scheme in combination with a range-separated hybrid functional appears to be a promising method for describing the ground and low-lying excited states of organic molecules on equal footing.

B. Comparison of *pp*-TDA and *hh*-TDA with linear response-type and full exchange response kernels

In this section, we compare the *hh*-TDA and *pp*-TDA schemes as well as the two different response kernel choices. In Table I, we have tabulated the statistical data for excitation energies computed for a subset of excitations from the Thiel benchmark set[81] with the linear response (LR) and HF-type kernels for *hh*-TDA-ωB97X and *pp*-TDA-PBE. We note that our *pp*-TDA-PBE (HF) results are in agreement with the ones presented earlier by Yang and co-workers (note that we use a slightly different basis set here).[45] The statistical data are listed in Table I, while detailed values of the individual systems and states are given in the supplementary material. A significant difference between the *hh*-TDA and *pp*-TDA schemes becomes apparent when looking at systems that involve both $\pi\pi^*$ and other types of excitations (i.e., $n\pi^*$ or $\sigma\pi^*$). Here, we find that *hh*-TDA typically provides the better option since the configuration space in *hh*-TDA is more suited to describe both excitation types simultaneously. This manifests itself in a larger number of states on this set, which can actually be described by *hh*-TDA. The nucleobases and carbonyl systems are particularly good cases for *hh*-TDA (see the supplementary material). For *pp*-TDA-PBE, SCF convergence problems for these systems eliminate the possibility to include them in the analysis. This seems to be due to (nearly) degenerate frontier molecular orbitals in the $(N-2)$ reference and was confirmed using alternative electronic structure software (Turbomole version 6.4).[74,92] The HF-type variant performs better for *pp*-TDA-PBE than the LR variant, the latter being equivalent to plain PBE orbital energy differences. For *hh*-TDA-ωB97X, this is reversed and the LR-type kernel performs better, as reflected by smaller mean (absolute) and standard deviations. Both *pp*-TDA-PBE schemes on average show underestimated excitation energies, whereas the opposite is true for *hh*-TDA-ωB97X. From all of the considered *pp*/*hh* schemes, *hh*-TDA-ωB97X (LR) performs the best on this set.

Compared to regular *ph*-TDA-ωB97X and EOM-CCSD, *hh*-TDA-ωB97X (LR) provides almost comparable accuracy, with a slightly less systematic error distribution as reflected by a SD, which is twice as large as for *ph*-TDA-ωB97X. In summary, we find that *hh*-TDA provides a reasonable method typically with a broader applicability to many organic systems compared to *pp*-TDA. In Sec. IV C, we will only consider the LR-type kernel variant of *hh*-TDA and investigate potential energy surface properties beyond the Franck–Condon point.

C. Potential energy surfaces with hh-TDA

1. Ethylene

As addressed in Sec. II D, one of the main advantages of the *hh*-TDA method is the ability to accurately treat degeneracies involving the ground state and low-lying excited states. The topologically correct description of the potential energy surfaces in regions of

TABLE I. Statistical data for excitation energies (in eV) computed with *hh*-TDA and *pp*-TDA using either the linear response (LR) type response kernel (this work) or the Hartree–Fock (HF) response kernel employed by Yang and co-workers. Particle–hole TD-DFT [Tamm–Dancoff approximated (TDA)] calculations and EOM-CCSD calculations are provided for comparison. All calculations use the spherical TZVP basis set. We chose DFAs which we expect to perform best for both schemes, i.e., a range-separated one for *hh*-TDA and a GGA for *pp*-TDA. The structures and reference values are taken from Ref. 81. If states could not be described by a method, they were discarded from the statistical analysis. The preceding PBE SCF calculations for the $(N-2)$-electron reference failed to converge for eight systems, precluding a total of 23 states to be considered for *pp*-TDA-PBE (see the supplementary material for details).

	EOM-CCSD	TDA-ωB97X	hh-TDA-ωB97X (LR)	hh-TDA-ωB97X (HF)	pp-TDA-PBE (LR)	pp-TDA-PBE (HF)
MD[a]	0.43	0.38	0.36	0.43	−0.25	−0.30
SD[b]	0.32	0.30	0.59	0.69	1.14	0.69
MAD[c]	0.44	0.40	0.54	0.67	0.98	0.59
States[d]	51	48	48	48	18	18

[a]Mean deviation.
[b]Standard deviation.
[c]Mean absolute deviation.
[d]Number of states included in the statistical data.

degeneracy is especially important in nonadiabatic photochemical dynamics where population transfer between adiabatic potential surfaces is often mediated by these seams of conical intersection. A prototypical example of such an intersection can be accessed through torsion and pyramidalization degrees of freedom in ethylene; this particular case has previously been used as a model system for assessing the ability of electronic structure methods to describe statically correlated character and ground-excited state degeneracies.[2]

Typical low-cost single reference excited state methods, such as CIS and TDDFT, suffer from instability related to HOMO–LUMO orbital degeneracies as an MECI involving the ground state and an excited state is approached. As a result, these methods cannot properly describe the twisted-pyramidalized MECI in ethylene. By contrast, *hh*-TDA is well-suited to describing conical intersection topologies, as demonstrated in combination with the ωB97X functional in Fig. 5(a), in which the double cone topology characterizes the vicinity of the S_0/S_1 MECI. Here, the potential energy surfaces are plotted along torsion and pyramidalization coordinates, which are the branching plane coordinates corresponding to the twisted-pyramidalized minimum energy conical intersection (MECI) between the S_0 ground state and the $\pi\pi^*$ excited state.

Moreover, CIS and TDDFT cannot describe double excitations, which then leads to a description of the S_1 minimum at a purely twisted geometry (90° torsion, no pyramidalization).[2] Methods that incorporate doubly excited states describe the S_1 minimum as simultaneously twisted (90° torsion) and pyramidalized. *hh*-TDA captures this feature of the S_1 potential energy surface (PES), as demonstrated by the appearance of the minimum at a twisted (90°) and pyramidalized (60°) geometry that lies 4.76 eV above the ground state minimum. This is detailed in Fig. 5(b). The S_1 minimum computed by the the-state-averaged, extended multi-state complete active space second-order perturbation method [SA3-XMS-CAS(2,2)PT2][93] on the same set of ethylene coordinates is found at 90° torsion and 72° pyramidalization and lies 5.46 eV above the ground state minimum [additional information regarding the SA3-XMS-CAS(2,2)PT2 comparison can be found in the supplementary material; these potential energy surfaces can be compared to previous results obtained with quasidegenerate multi-reference perturbation theory[2]]. These results indicate that *hh*-TDA describes the potential energy surfaces reasonably well and thus is a promising candidate for applications in efficient nonadiabatic dynamics simulations. This finding complements earlier studies on H_3 and NH_3, which showed that *pp*-TDA is able to describe conical interactions.[53]

2. Thymine

The thymine molecule is a biologically relevant prototype for internal conversion dynamics between $n\pi^*$ and $\pi\pi^*$ states. At the Franck–Condon point, highly accurate coupled cluster (CC) computations predict that thymine has nearly degenerate S_1 and S_2 states of $n\pi^*$ and $\pi\pi^*$ character, respectively.[86] Furthermore, accurate CC-based methods predict a reaction coordinate from the Franck–Condon point to the MECI between the S_1 and S_2 states without barriers or the presence of minima on the S_2 state.[86] At lower levels of theory—particularly those that do not include dynamic electron correlation, such as CASSCF—it is common to find a larger (greater than 1 eV) splitting between the S_1 and S_2 states at the Franck–Condon point as well as a minimum on the S_2 state.[94,95] It

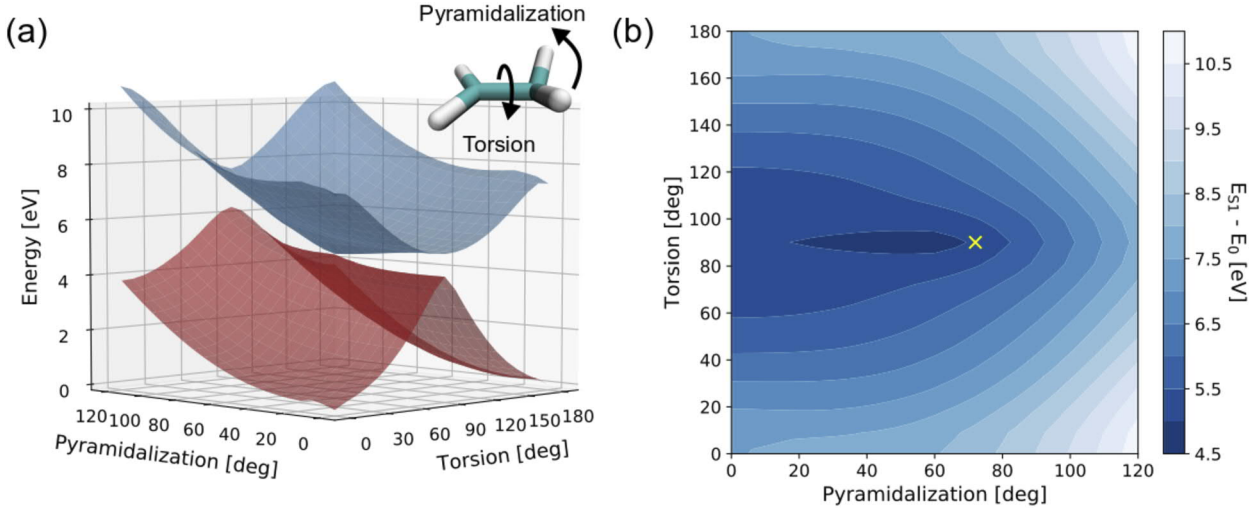

FIG. 5. (a) Global features of the S_0 ground (red) and S_1 excited (blue) state PESs of ethylene computed at the *hh*-TDA-ωB97X/def2-SVP level in a rigid scan over the branching plane coordinates of pyramidalization and torsion (visualized in the inset). The linear response-type kernel has been employed. *hh*-TDA describes the S_0/S_1 degeneracy in ethylene, as demonstrated here with the appearance of the double cone feature. Ethylene reaches the conical intersection geometry once distorted to 90° torsion and at 60° pyramidalization. This point coincides with the predicted S_1 minimum, lying 4.76 eV above the ground state minimum. (b) The S_1 PES from (a) represented as a contour plot. The shape of the S_1 PES is relatively well-described by *hh*-TDA-ωB97X compared to previously reported quasidegenerate multi-reference perturbation theory results.[2] The S_1 minimum appears at a simultaneously twisted and pyramidalized geometry. For comparison, the location of the S_1 minimum obtained from SA3-XMS-CAS(2,2)PT2 (see the supplementary material for details) that lies 5.46 eV above the S_0 ground state is marked by a light-yellow X.

remains unclear how these properties of the thymine PES affect its photodynamics; highly efficient electronic structure methods that agree more closely with the accurate CC-based methods would be required to answer these questions. We find *hh*-TDA to be a promising candidate for use in nonadiabatic dynamics simulations of thymine.

The relative excited state energies computed with *hh*-TDA with the ωPBE(ω = 0.2 au) functional and EOM-CCSD (see Sec. III) at three different thymine structures are shown in Fig. 6. The vertical excitation energies to the S_1 and S_2 states are underestimated by about 0.5 eV–0.8 eV by *hh*-TDA-ωPBE(ω = 0.2 a.u.) compared to EOM-CCSD. The latter themselves are, however, higher by about 0.2 eV–0.3 eV compared to the higher-level CC3 data.[86] The S_1/S_2 splittings are reproduced to within 0.17 eV–0.22 eV by *hh*-TDA. As a result, *hh*-TDA does a particularly good job describing the relative energetics of the S_1 and S_2 states at stationary points relevant to the photodynamics of thymine. The stabilization of the S_1 ($n\pi^*$) minimum is correct to 0.04 eV compared to both the Franck–Condon point and S_1/S_2 MECI. Furthermore, no minimum is present on the S_2 PES of thymine between the Franck–Condon point and S_1/S_2 MECI. The relative energy of that intersection with respect to the S_2 energy at the Franck–Condon point is also in good agreement with EOM-CCSD. Remembering that the computational cost of *hh*-TDA scales formally as $O(N^4)$ but, in practice, as $O(N^2)$ with system size (see Sec. IV D), while EOM-CCSD formally scales as $O(N^6)$, the agreement between these methods is quite remarkable. What remains to be done in the future studies is to apply *hh*-TDA directly in a nonadiabatic dynamics simulation of thymine and assess the performance against experimental ultrafast spectroscopic observables.

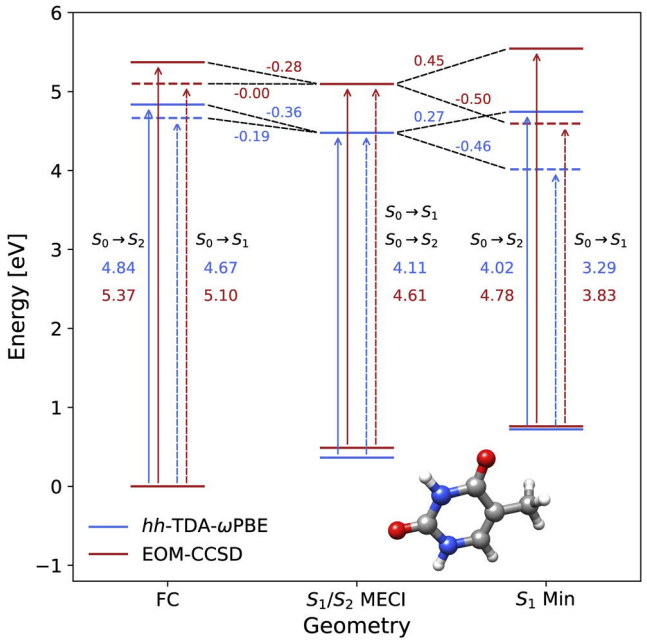

FIG. 6. Relative energies (in eV) of the lowest three singlet electronic states of thymine computed at the *hh*-TDA-ωPBE(ω = 0.2 a.u.)/6-31G** (blue) and EOM-CCSD/aug-cc-pVDZ (red) levels of theory. Energies are computed at three critical points relevant to the excited state dynamics of thymine: the S_0 minimum (FC), the minimum energy conical intersection between the S_1 and S_2 states (S_1/S_2 MECI), and the S_1 minimum (S_1 min). The arrows indicate vertical excitations to S_2 (solid) and S_1 (dashed). Geometries are optimized for *hh*-TDA and taken from Ref. 86 for EOM-CCSD (see Sec. III for technical details). All energies are given relative to the respective S_0 energy at the Franck–Condon point. Higher level vertical excitation energies at the CC3 level of theory are 0.20 eV–0.26 eV lower compared to our EOM-CCSD/aug-cc-pVDZ (cf. Ref. 86) and thus in better agreement with the *hh*-TDA-ωPBE(ω = 0.2 a.u.)/6-31G** results.

3. Malonaldehyde

Malonaldehyde is a molecule that is a prototype for excited-state proton transfer, $n\pi^*/\pi\pi^*$ internal conversion dynamics, and photoisomerization. Here, we apply *hh*-TDA with the ωB97[76] functional and compare to the results obtained with multireference configuration interaction methods including single and double excitations (MRSDCI, see Fig. 7).[87] Again, we find good agreement in the absolute excitation energies and in the splitting between $n\pi^*$ and $\pi\pi^*$ states at the Franck–Condon point. However, the relative energetics of the S_1 and S_2 states at important stationary points show some potential problems. The minimum on the S_1 ($n\pi^*$) state is a bit too stable relative to both the Franck–Condon point and the S_0/S_1 MECI. This indicates that the population may become spuriously trapped on the S_1 state leading to longer excited-state lifetimes and perhaps increased involvement of triplet states (in view of the El-Sayed rules and the fact that the electronic wavefunction has $n\pi^*$ character in the region). In addition, the S_1/S_2 MECI reached by proton transfer is energetically unfavorable. This may indicate that the proton transfer reaction will play a different role in the internal conversion dynamics than MRSDCI would predict. The issues encountered by *hh*-TDA for malonaldehyde seem to be related to the restriction on the orbital space to include only one π^* orbital. For this molecule, a second π^* orbital may be essential to an accurate description of the photodynamics. Although we expect that malonaldehyde is not an ideal application of the *hh*-TDA method, nonadiabatic dynamics simulations, in which the molecular symmetry is lifted, would provide a more definitive assessment of the performance of *hh*-TDA for this molecule.

D. Computational cost of *hh*-TDA

In Fig. 8, we report the computational time required to solve for the ground and first excited state of the Nile blue chromophore in aqueous solution using the *hh*-TDA and TDA-TDDFT methods with the Cartesian def2-SVP basis set and the ωPBE functional with ω = 0.8 a.u. The principal conclusions that should be drawn from these timings are that the *hh*-TDA and TDA-TDDFT methods are of similar computational cost and exhibit similar scaling behavior with the system size, i.e., $O(N^2)$ in our AO direct implementation (see below). In TDDFT, the solution of the KS equations defines the ground state, whereas in *hh*-TDA, both the ground and excited states are obtained as eigenvectors of the TDA response matrix. We find that multiplication of trial vectors against the response matrix is less expensive in the *hh*-TDA method (because there are no contributions from the Coulomb-type integrals or derivatives of the exchange-correlation potential). In cases where only one or two excited states are required, it should be expected that the cost of

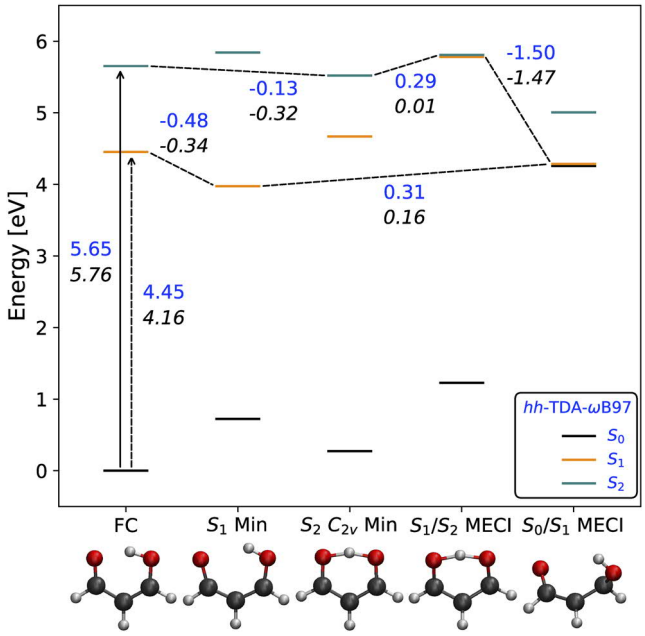

FIG. 7. Relative energies (in eV) of the lowest three singlet electronic states of malonaldehyde for critical geometries computed at the *hh*-TDA-ωB97/6-31G** (blue normal print) and MRSDCI/6-31G*//SA3-CAS(4,4)SCF/6-31G* (black italics, taken from Ref. 87) levels of theory. In the latter, all configurations generated in a (4,4) active space served as references in the MRSDCI calculations. The Franck–Condon, S_1 minimum, and S_0/S_1 minimum energy conical intersection geometries are optimized without constraints. The S_2 C_{2v} minimum and S_1/S_2 MECI are minima in the C_{2v} and C_s point groups, respectively. Only the energy levels computed at the *hh*-TDA-ωB97/6-31G** level of theory are plotted, and the vertical excitations at the Franck–Condon point to S_2 and S_1 are illustrated as solid and dashed arrows, respectively.

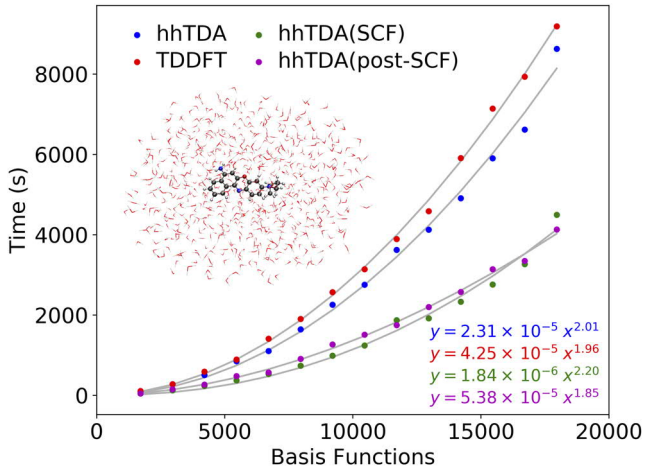

FIG. 8. Timings of *hh*-TDA/def2-SVP and TDA-TDDFT/def2-SVP computations of the ground and first excited state of Nile blue including microsolvation by 50–700 water molecules. The *hh*-TDA/def2-SVP computation is decomposed into the time spent in the KS SCF for the (N+2)-electron system and the "post-SCF" portion of the computation that comprises the Davidson diagonalization to obtain the lowest two eigenpairs as defined in Eq. (18). The largest system considered contained more than 2100 atoms and nearly 18 000 basis functions. The timings were performed using eight NVIDIA V100 GPUs and eight Intel Xeon E5-2698 CPU cores clocked at 2.2 GHz. Best fit power series are given for each of the methods. For both methods, the ωPBE functional with a range-separation parameter of 0.8 a.u. was used.

TDA-TDDFT and *hh*-TDA will be quite similar, with the particulars of a given molecule determining which method will be faster. For example, in the present case, TDDFT required extra guess vectors in the Davidson diagonalization in order to avoid solving for higher-lying charge transfer excited states rather than the locally excited state of Nile blue.

Formally, the *hh*-TDA method appears to scale as $O(o^6)$, where o represents the number of occupied orbitals. However, since only a few electronic states are actually of interest, the full diagonalization of the response matrix can be avoided, and the scaling of the method would be $O(o^4)$—the cost of the multiplication of a trial vector by the response matrix. However, this ignores the cost of forming the response matrix in the molecular orbital basis. In practice, our implementation of *hh*-TDA is fully AO integral direct and scales, formally, as $O(N^4)$, where N is the number of AO basis functions. The advantage of the AO formulation of *hh*-TDA is that sparsity can be exploited and the contractions between trial vectors and the response matrix scale more like $O(N^2)$. This is clearly demonstrated in Fig. 8, where the apparent quadratic scaling of the method allows us to apply it to systems with more than 2100 atoms in a polarized double-ζ basis set (roughly 18 000 basis functions). It should be noted that the underlying SCF procedure costs approximately the same as the solution of the eigenvalue problem (for two states) and the SCF procedure scales slightly worse with the system size.

E. The unbound orbital problem and basis set requirements

Following the remarks above on the basis set requirements for *hh*-TDA due to the (N+2)-electron reference, all calculations in this paper used double- and triple-zeta basis sets without diffuse functions. In order to explore the basis set dependence more thoroughly, we collect the lowest excitation energies computed with *hh*-TDA-ωB97X and different basis sets STO-3G, def2-SVP, def2-SVPD, def2-TZVP, and def2-QZVP (the latter two without f and g functions) for a few molecular systems (acetamide, *p*-benzoquinone, butadiene, ethylene, formaldehyde, norbornadiene, uracil, and water) in Table S11 of the supplementary material. As could be expected, these results show that excitation energies obtained with the STO-3G basis set are widely disparate from larger basis sets. However, with the exception of acetamide, the excitation energies vary mostly by less than 0.2 eV over the other choices of basis sets without diffuse functions. This indicates that the presence of unbound orbitals need not be a significant problem (as long as diffuse basis sets are avoided, see results for def2-SVPD).

Acetamide was among the problematic systems mentioned in Sec. IV A, where DFAs with insufficient exact exchange populated an incorrect orbital in the (N+2)-electron reference. Similar occupation problems are observed for the def2 basis sets considered here, leading to strong basis set dependence of the excitation energy. However, this seems to be distinct from the unbound

orbital problem and is instead related to the limited active space in *hh*-TDA.

Based on this assessment and the promising results obtained in this work, we therefore recommend the use of *hh*-TDA in combination with asymptotically correct range-separated hybrid DFAs and double- and triple-zeta basis sets without diffuse basis functions. The latter can be added if the excited states to be probed by *hh*-TDA are actually of Rydberg character (cf. results for water). In the future, the unbound orbital issue could be addressed by using an N-electron reference in the orbital generation. Such an approach was already applied in one of the early works on *pp*-RPA.[49] We plan to investigate this issue in order to facilitate the routine use of *hh*-TDA in geometry optimizations and nonadiabatic dynamics simulations.

V. CONCLUSIONS

We have shown that the hole–hole Tamm–Dancoff approximation (*hh*-TDA) to the particle–particle random-phase approximation (*pp*-RPA) represents an efficient DFT-based electronic structure scheme for the electronic ground and low-lying excited states. The method shares similarities with the previously presented particle–particle (*pp*-TDA) approach. We find some advantages of the *hh*-TDA scheme, particularly in its ability to describe different low-lying excitation types ($n\pi^*$, $\sigma\pi^*$, and $\pi\pi^*$). Starting from an (N+2)-electron reference determinant, the ground and the low-lying excited states of the N-electron target system are obtained by a double annihilation of two electrons. Since the ground and excited states are obtained from the same eigenvalue problem, static correlation cases can be handled. Dynamic correlation is included in the orbitals by virtue of the density functional. We have also introduced an alternative choice for the response kernel that differs from the functional-independent Hartree–Fock-type kernel employed in the previous works on *pp*-RPA and *pp*-TDA.[54] Our choice is functional-dependent and in line with the response kernels appearing in particle–hole linear response theory.

To avoid SCF convergence problems of the (N+2)-electron reference, the method should be combined with range-separated density functionals that have 100% asymptotic Fock exchange. We recommend avoidance of diffuse atom-centered basis sets since these can lead to continuum-like orbitals in the (N+2)-electron reference. We then do not observe any SCF convergence problems and find that the *hh*-TDA can describe low-lying excited states reasonably well at a computational complexity comparable to a configuration interaction singles (CIS) calculation. As with any density functional approximation-based method, case-specific functional assessment is recommended. The range-separation parameter and amount of short-range Fock exchange can be viewed as parameters to optimize the method performance for a specific molecule (as is often done by variation of the active space in CAS methods).

On the other hand, the main limitation of the *hh*-TDA is the restricted "virtual" orbital space, which formally consists exclusively of the lowest unoccupied orbital (with respect to the N-electron system). This precludes its application to systems with degenerate LUMOs, such as benzene. In spite of this shortcoming, the *hh*-TDA method is well-suited for the calculation of ground and low-lying excited states for many organic molecules. It offers an inexpensive alternative to the existing and widely used CASSCF methods, with the advantage that dynamic correlation effects are included at the orbital level by means of the used density functional.

The method is implemented in the GPU-accelerated electronic structure code TeraChem. Future directions will include the computation of nonadiabatic couplings and testing the method in nonadiabatic dynamics simulations. In this context, it will be important to address the problem of potentially occupying unbound orbitals in the (N+2)-electron SCF calculation. Generating orbitals for an N-electron reference with fractional orbital occupation and using them in an (N+2)-electron-type *hh*-TDA procedure could remove this issue entirely, while guaranteeing stability in nonadiabatic dynamics simulations. This will be explored in the future work.

SUPPLEMENTAL MATERIAL

See the supplementary material for a zip-file containing *hh*-TDA optimized geometries of thymine (Fig. 6) and malonaldehyde (Fig. 7) and a pdf file containing detailed results on the DFA assessment (Sec. IV A) and the *pp*/*hh*-TDA benchmarks (Sec. IV B) and a potential curve of ethylene (at 90° torsion).

ACKNOWLEDGMENTS

This work was supported by the AMOS program of the U.S. Department of Energy, Office of Science, Basic Energy Sciences, Chemical Sciences, and Biosciences Division and by the Department of Energy, Laboratory Directed Research and Development program at the SLAC National Accelerator Laboratory under Contract No. DE-AC02-76SF00515. T.J.M. is a co-founder of PetaChem, LLC. C.B. thanks the German National Academy of Sciences Leopoldina for support through the Leopoldina Fellowship Program (Project No. LPDS 2018-09). The authors thank Deniz Tuna for helpful discussions and for early testing of the method.

DATA AVAILABILITY

The data that support the findings of this study are available from the corresponding author upon reasonable request.

REFERENCES

[1] A. Dreuw and M. Head-Gordon, "Single-reference *ab initio* methods for the calculation of excited states of large molecules," Chem. Rev. **105**, 4009–4037 (2005).

[2] B. G. Levine, C. Ko, J. Quenneville, and T. J. Martínez, "Conical intersections and double excitations in time-dependent density functional theory," Mol. Phys. **104**, 1039–1051 (2006).

[3] B. O. Roos, "The complete active space SCF method in a fock-matrix-based super-CI formulation," Int. J. Quantum Chem. **18**, 175–189 (1980).

[4] B. O. Roos, "Theoretical studies of electronically excited states of molecular systems using multiconfigurational perturbation theory," Acc. Chem. Res. **32**, 137–144 (1999).

[5] H. J. Werner and P. J. Knowles, "An efficient internally contracted multiconfiguration reference configuration-interaction method," J. Chem. Phys. **89**, 5803–5814 (1988).

[6] J. D. Coe, B. G. Levine, and T. J. Martínez, "*Ab initio* molecular dynamics of excited state intramolecular proton transfer using multireference perturbation theory," J. Phys. Chem. A **111**, 11302–11310 (2007).

[7]H. Tao, B. G. Levine, and T. J. Martínez, "*Ab initio* multiple spawning dynamics using multi-state second-order perturbation theory," J. Phys. Chem. A **113**, 13656–13662 (2009).
[8]H. Tao, T. K. Allison, T. W. Wright, A. M. Stooke, C. Khurmi, J. van Tilborg, Y. Liu, R. W. Falcone, A. Belkacem, and T. J. Martinez, "Ultrafast internal conversion in ethylene. I. The excited state lifetime," J. Chem. Phys. **134**, 244306 (2011).
[9]T. Mori, W. J. Glover, M. S. Schuurman, and T. J. Martinez, "Role of Rydberg states in the photochemical dynamics of ethylene," J. Phys. Chem. A **116**, 2808–2818 (2012).
[10]L. Liu, J. Liu, and T. J. Martinez, "Dynamical correlation effects on photoisomerization: *Ab initio* multiple spawning dynamics with MS-CASPT2 for a model trans-protonated schiff base," J. Phys. Chem. B **120**, 1940–1949 (2016).
[11]J. W. Park and T. Shiozaki, "On-the-fly CASPT2 surface-hopping dynamics," J. Chem. Theory Comput. **13**, 3676–3683 (2017).
[12]W. J. Glover, T. Mori, M. S. Schuurman, A. E. Boguslavskiy, O. Schalk, A. Stolow, and T. J. Martínez, "Excited state non-adiabatic dynamics of the smallest polyene, trans 1,3-butadiene. II. *Ab initio* multiple spawning simulations," J. Chem. Phys. **148**, 164303 (2018).
[13]J. W. Snyder, R. M. Parrish, and T. J. Martínez, "α-CASSCF: An efficient, empirical correction for SA-CASSCF to closely approximate MS-CASPT2 potential energy surfaces," J. Phys. Chem. Lett. **8**, 2432–2437 (2017).
[14]A. Koslowski, M. E. Beck, and W. Thiel, "Implementation of a general multireference configuration interaction procedure with analytic gradients in a semiempirical context using the graphical unitary group approach," J. Comput. Chem. **24**, 714–726 (2003).
[15]A. Toniolo, A. L. Thompson, and T. J. Martínez, "Excited state direct dynamics of benzene with reparameterized multi-reference semiempirical configuration interaction methods," Chem. Phys. **304**, 133–145 (2004).
[16]A. Toniolo, G. Granucci, S. Inglese, and M. Persico, "Theoretical study of the photodissociation dynamics of ClOOCl," Phys. Chem. Chem. Phys. **3**, 4266–4279 (2001).
[17]K. Sastry, D. D. Johnson, A. L. Thompson, D. E. Goldberg, T. J. Martinez, J. Leiding, and J. Owens, "Optimization of semiempirical quantum chemistry methods via multiobjective genetic algorithms: Accurate photodynamics for larger molecules and longer time scales," Mater. Manuf. Processes **22**, 553–561 (2007).
[18]S. Ghosh, P. Verma, C. J. Cramer, L. Gagliardi, and D. G. Truhlar, "Combining wave function methods with density functional theory for excited states," Chem. Rev. **118**, 7249–7292 (2018).
[19]S. Pijeau and E. G. Hohenstein, "Improved complete active space configuration interaction energies with a simple correction from density functional theory," J. Chem. Theory Comput. **13**, 1130–1146 (2017).
[20]B. Miehlich, H. Stoll, and A. Savin, "A correlation-energy density functional for multideterminantal wavefunctions," Mol. Phys. **91**, 527–536 (1997).
[21]C. Gutle and A. Savin, "Orbital spaces and density-functional theory," Phys. Rev. A **75**, 032519 (2007).
[22]L. Gagliardi, D. G. Truhlar, G. Li Manni, R. K. Carlson, C. E. Hoyer, and J. W. L. Bao, "Multiconfiguration pair-density functional theory: A new way to treat strongly correlated systems," Acc. Chem. Res. **50**, 66–73 (2017).
[23]A. M. Sand, C. E. Hoyer, D. G. Truhlar, and L. Gagliardi, "State-interaction pair-density functional theory," J. Chem. Phys. **149**, 024106 (2018).
[24]S. L. Li, A. V. Marenich, X. Xu, and D. G. Truhlar, "Configuration interaction-corrected Tamm–Dancoff approximation: A time-dependent density functional method with the correct dimensionality of conical intersections," J. Phys. Chem. Lett. **5**, 322–328 (2014).
[25]H.-H. Teh and J. E. Subotnik, "The simplest possible approach for simulating S_0–S_1 conical intersections with DFT/TDDFT: Adding one doubly excited configuration," J. Phys. Chem. Lett. **10**, 3426–3432 (2019).
[26]S. Grimme and M. Waletzke, "A combination of Kohn–Sham density functional theory and multi-reference configuration interaction methods," J. Chem. Phys. **111**, 5645–5655 (1999).
[27]C. M. Marian, A. Heil, and M. Kleinschmidt, "The DFT/MRCI method," Wiley Interdiscip. Rev.: Comput. Mol. Sci. **9**, e1394 (2019).
[28]Y. Shu, K. A. Parker, and D. G. Truhlar, "Dual-functional Tamm–Dancoff approximation: A convenient density functional method that correctly describes S_1/S_0 conical intersections," J. Phys. Chem. Lett. **8**, 2107–2112 (2017).
[29]A. I. Krylov, Y. Shao, and M. Head-Gordon, "The spin–flip approach within time-dependent density functional theory: Theory and applications to diradicals," J. Chem. Phys. **118**, 4807–4818 (2003).
[30]J. S. Sears, C. D. Sherrill, and A. I. Krylov, "A spin-complete version of the spin-flip approach to bond breaking: What is the impact of obtaining spin eigenfunctions?," J. Chem. Phys. **118**, 9084–9094 (2003).
[31]D. Casanova and M. Head-Gordon, "The spin-flip extended single excitation configuration interaction method," J. Chem. Phys. **129**, 064104 (2008).
[32]X. Zhang and J. M. Herbert, "Spin-flip, tensor equation-of-motion configuration interaction with a density-functional correction: A spin-complete method for exploring excited-state potential energy surfaces," J. Chem. Phys. **143**, 234107 (2015).
[33]M. Filatov, "Spin-restricted ensemble-referenced Kohn–Sham method: Basic principles and application to strongly correlated ground and excited states of molecules," Wiley Interdiscip. Rev.: Comput. Mol. Sci. **5**, 146–167 (2015).
[34]M. Filatov, F. Liu, and T. J. Martínez, "Analytical derivatives of the individual state energies in ensemble density functional theory method. I. General formalism," J. Chem. Phys. **147**, 034113 (2017).
[35]F. Liu, M. Filatov, and T. J. Martínez, "Analytical derivatives of the individual state energies in ensemble density functional theory method: II. Implementation on graphical processing units (GPUs)," ChemRxiv (published online 2019).
[36]D. Peng, S. N. Steinmann, H. van Aggelen, and W. Yang, "Equivalence of particle–particle random phase approximation correlation energy and ladder-coupled-cluster doubles," J. Chem. Phys. **139**, 104112 (2013).
[37]H. van Aggelen, Y. Yang, and W. Yang, "Exchange-correlation energy from pairing matrix fluctuation and the particle–particle random-phase approximation," Phys. Rev. A **88**, 030501 (2013).
[38]H. van Aggelen, Y. Yang, and W. Yang, "Exchange-correlation energy from pairing matrix fluctuation and the particle–particle random phase approximation," J. Chem. Phys. **140**, 18A511 (2014).
[39]Y. Yang, H. van Aggelen, S. N. Steinmann, D. Peng, and W. Yang, "Benchmark tests and spin adaptation for the particle–particle random phase approximation," J. Chem. Phys. **139**, 174110 (2013).
[40]N. Shenvi, H. van Aggelen, Y. Yang, and W. Yang, "Tensor hypercontracted ppRPA: Reducing the cost of the particle-particle random phase approximation from O(r 6) to O(r 4)," J. Chem. Phys. **141**, 024119 (2014).
[41]G. E. Scuseria, T. M. Henderson, and I. W. Bulik, "Particle–particle and quasiparticle random phase approximations: Connections to coupled cluster theory," J. Chem. Phys. **139**, 104113 (2013).
[42]G. E. Scuseria, T. M. Henderson, and D. C. Sorensen, "The ground state correlation energy of the random phase approximation from a ring coupled cluster doubles approach," J. Chem. Phys. **129**, 231101 (2008).
[43]R. Al-Saadon, C. Sutton, and W. Yang, "Accurate treatment of charge-transfer excitations and thermally activated delayed fluorescence using the particle–particle random phase approximation," J. Chem. Theory Comput. **14**, 3196–3204 (2018).
[44]Y. Jin, Y. Yang, D. Zhang, D. Peng, and W. Yang, "Excitation energies from particle–particle random phase approximation with accurate optimized effective potentials," J. Chem. Phys. **147**, 134105 (2017).
[45]Y. Yang, D. Peng, J. Lu, and W. Yang, "Excitation energies from particle–particle random phase approximation: Davidson algorithm and benchmark studies," J. Chem. Phys. **141**, 124104 (2014).
[46]C. Sutton, Y. Yang, D. Zhang, and W. Yang, "Single, double electronic excitations and exciton effective conjugation lengths in π-conjugated systems," J. Phys. Chem. Lett. **9**, 4029–4036 (2018).
[47]Y. Yang, A. Dominguez, D. Zhang, V. Lutsker, T. A. Niehaus, T. Frauenheim, and W. Yang, "Charge transfer excitations from particle–particle random phase approximation—Opportunities and challenges arising from two-electron deficient systems," J. Chem. Phys. **146**, 124104 (2017).
[48]Y. Yang, D. Peng, E. R. Davidson, and W. Yang, "Singlet–triplet energy gaps for diradicals from particle–particle random phase approximation," J. Phys. Chem. A **119**, 4923–4932 (2015).

[49]Y. Yang, H. van Aggelen, and W. Yang, "Double, Rydberg and charge transfer excitations from pairing matrix fluctuation and particle–particle random phase approximation," J. Chem. Phys. **139**, 224105 (2013).
[50]D. Zhang, D. Peng, P. Zhang, and W. Yang, "Analytic gradients, geometry optimization and excited state potential energy surfaces from the particle–particle random phase approximation," Phys. Chem. Chem. Phys. **17**, 1025–1038 (2015).
[51]B. Pinter, R. Al-Saadon, Z. Chen, and W. Yang, "Spin-state energetics of iron(II) porphyrin from the particle–particle random phase approximation," Eur. Phys. J. B **91**, 270 (2018).
[52]Y. Yang, E. R. Davidson, and W. Yang, "Nature of ground and electronic excited states of higher acenes," Proc. Natl. Acad. Sci. U. S. A. **113**, E5098 (2016).
[53]Y. Yang, L. Shen, D. Zhang, and W. Yang, "Conical intersections from particle–particle random phase and Tamm–Dancoff approximations," J. Phys. Chem. Lett. **7**, 2407–2411 (2016).
[54]D. Peng, H. van Aggelen, Y. Yang, and W. Yang, "Linear-response time-dependent density-functional theory with pairing fields," J. Chem. Phys. **140**, 18A522 (2014).
[55]L. N. Oliveira, E. K. U. Gross, and W. Kohn, "Density-functional theory for superconductors," Phys. Rev. Lett. **60**, 2430–2433 (1988).
[56]E. K. U. Gross and S. Kurth, "Density-functional theory of the superconducting state," Int. J. Quantum Chem. **40**, 289–297 (1991).
[57]M. Lüders, M. A. L. Marques, N. N. Lathiotakis, A. Floris, G. Profeta, L. Fast, A. Continenza, S. Massidda, and E. K. U. Gross, "*Ab initio* theory of superconductivity. I. Density functional formalism and approximate functionals," Phys. Rev. B **72**, 024545 (2005).
[58]M. E. Casida, *Time-Dependent Density Functional Response Theory for Molecules in: Recent Advances in Density Functional Methods*, edited by D. P. Chong (World Scientific, Singapore, 1995), Vol. 1.
[59]A. Köhn and A. Tajti, "Can coupled-cluster theory treat conical intersections?," J. Chem. Phys. **127**, 044105 (2007).
[60]E. F. Kjønstad, R. H. Myhre, T. J. Martínez, and H. Koch, "Crossing conditions in coupled cluster theory," J. Chem. Phys. **147**, 164105 (2017).
[61]J. C. Rienstra-Kiracofe, G. S. Tschumper, H. F. Schaefer, S. Nandi, and G. B. Ellison, "Atomic and molecular electron affinities: Photoelectron experiments and theoretical computations," Chem. Rev. **102**, 231–282 (2002).
[62]J. P. Perdew, W. Yang, K. Burke, Z. Yang, E. K. U. Gross, M. Scheffler, G. E. Scuseria, T. M. Henderson, I. Y. Zhang, A. Ruzsinszky, H. Peng, J. Sun, E. Trushin, and A. Görling, "Understanding band gaps of solids in generalized Kohn–Sham theory," Proc. Natl. Acad. Sci. U. S. A. **114**, 2801 (2017).
[63]E. J. Baerends, O. V. Gritsenko, and R. van Meer, "The Kohn–Sham gap, the fundamental gap and the optical gap: The physical meaning of occupied and virtual Kohn–Sham orbital energies," Phys. Chem. Chem. Phys. **15**, 16408–16425 (2013).
[64]I. S. Ufimtsev and T. J. Martínez, "Quantum chemistry on graphical processing units. 1. Strategies for two-electron integral evaluation," J. Chem. Theory Comput. **4**, 222–231 (2008).
[65]I. S. Ufimtsev and T. J. Martinez, "Quantum chemistry on graphical processing units. 2. Direct self-consistent-field implementation," J. Chem. Theory Comput. **5**, 1004–1015 (2009).
[66]A. D. Becke, "Density-functional exchange-energy approximation with correct asymptotic behaviour," Phys. Rev. A **38**, 3098–3100 (1988).
[67]C. Lee, W. Yang, and R. G. Parr, "Development of the Colle–Salvetti correlation-energy formula into a functional of the electron density," Phys. Rev. B **37**, 785–789 (1988).
[68]A. D. Becke, "Density-functional thermochemistry. III. The role of exact exchange," J. Chem. Phys. **98**, 5648–5652 (1993).
[69]P. J. Stephens, F. J. Devlin, C. F. Chabalowski, and M. J. Frisch, "*Ab initio* calculation of vibrational absorption and circular Dichroism spectra using density functional force fields," J. Phys. Chem. **98**, 11623–11627 (1994).
[70]J. P. Perdew, K. Burke, and M. Ernzerhof, "Generalized gradient approximation made simple," Phys. Rev. Lett. **77**, 3865–3868 (1996).
[71]C. Adamo and V. Barone, "Toward reliable density functional methods without adjustable parameters: The PBE0 model," J. Chem. Phys. **110**, 6158–6170 (1999).
[72]A. D. Becke, "A new mixing of Hartree–Fock and local density-functional theories," J. Chem. Phys. **98**, 1372–1377 (1993).
[73]T. Yanai, D. P. Tew, and N. C. Handy, "A new hybrid exchange–correlation functional using the Coulomb–attenuating method (CAM-B3LYP)," Chem. Phys. Lett. **393**, 51–57 (2004).
[74]M. A. Rohrdanz, K. M. Martins, and J. M. Herbert, "A long-range-corrected density functional that performs well for both ground-state properties and time-dependent density functional theory excitation energies, including charge-transfer excited states," J. Chem. Phys. **130**, 054112 (2009).
[75]A. D. Becke, "Density-functional thermochemistry. V. Systematic optimization of exchange-correlation functionals," J. Chem. Phys. **107**, 8554–8560 (1997).
[76]J.-D. Chai and M. Head-Gordon, "Systematic optimization of long-range corrected hybrid density functionals," J. Chem. Phys. **128**, 084106 (2008).
[77]Y.-S. Lin, G.-D. Li, S.-P. Mao, and J.-D. Chai, "Long-range corrected hybrid density functionals with improved dispersion corrections," J. Chem. Theory Comput. **9**, 263–272 (2013).
[78]A. Schäfer, H. Horn, and R. Ahlrichs, "Fully optimized contracted Gaussian basis sets for atoms Li to Kr," J. Chem. Phys. **97**, 2571–2577 (1992).
[79]F. Weigend and R. Ahlrichs, "Balanced basis sets of split valence, triple zeta valence and quadruple zeta valence quality for H to Rn: Design and assessment of accuracy," Phys. Chem. Chem. Phys. **7**, 3297–3305 (2005).
[80]A. Schäfer, C. Huber, and R. Ahlrichs, "Fully optimized contracted Gaussian basis sets of triple zeta valence quality for atoms Li to Kr," J. Chem. Phys. **100**, 5829–5835 (1994).
[81]M. Schreiber, M. R. Silva-Junior, S. P. A. Sauer, and W. Thiel, "Benchmarks for electronically excited states: CASPT2, CC2, CCSD, and CC3," J. Chem. Phys. **128**, 134110 (2008).
[82]Y. Shao, Z. Gan, E. Epifanovsky, A. T. B. Gilbert, M. Wormit, J. Kussmann, A. W. Lange, A. Behn, J. Deng, X. Feng, D. Ghosh, M. Goldey, P. R. Horn, L. D. Jacobson, I. Kaliman, R. Z. Khaliullin, T. Kuś, A. Landau, J. Liu, E. I. Proynov, Y. M. Rhee, R. M. Richard, M. A. Rohrdanz, R. P. Steele, E. J. Sundstrom, H. L. Woodcock, P. M. Zimmerman, D. Zuev, B. Albrecht, E. Alguire, B. Austin, G. J. O. Beran, Y. A. Bernard, E. Berquist, K. Brandhorst, K. B. Bravaya, S. T. Brown, D. Casanova, C.-M. Chang, Y. Chen, S. H. Chien, K. D. Closser, D. L. Crittenden, M. Diedenhofen, R. A. DiStasio, H. Do, A. D. Dutoi, R. G. Edgar, S. Fatehi, L. Fusti-Molnar, A. Ghysels, A. Golubeva-Zadorozhnaya, J. Gomes, M. W. D. Hanson-Heine, P. H. P. Harbach, A. W. Hauser, E. G. Hohenstein, Z. C. Holden, T.-C. Jagau, H. Ji, B. Kaduk, K. Khistyaev, J. Kim, J. Kim, R. A. King, P. Klunzinger, D. Kosenkov, T. Kowalczyk, C. M. Krauter, K. U. Lao, A. D. Laurent, K. V. Lawler, S. V. Levchenko, C. Y. Lin, F. Liu, E. Livshits, R. C. Lochan, A. Luenser, P. Manohar, S. F. Manzer, S.-P. Mao, N. Mardirossian, A. V. Marenich, S. A. Maurer, N. J. Mayhall, E. Neuscamman, C. M. Oana, R. Olivares-Amaya, D. P. O'Neill, J. A. Parkhill, T. M. Perrine, R. Peverati, A. Prociuk, D. R. Rehn, E. Rosta, N. J. Russ, S. M. Sharada, S. Sharma, D. W. Small, A. Sodt, T. Stein, D. Stück, Y.-C. Su, A. J. W. Thom, T. Tsuchimochi, V. Vanovschi, L. Vogt, O. Vydrov, T. Wang, M. A. Watson, J. Wenzel, A. White, C. F. Williams, J. Yang, S. Yeganeh, S. R. Yost, Z.-Q. You, I. Y. Zhang, X. Zhang, Y. Zhao, B. R. Brooks, G. K. L. Chan, D. M. Chipman, C. J. Cramer, W. A. Goddard, M. S. Gordon, W. J. Hehre, A. Klamt, H. F. Schaefer, M. W. Schmidt, C. D. Sherrill, D. G. Truhlar, A. Warshel, X. Xu, A. Aspuru-Guzik, R. Baer, A. T. Bell, N. A. Besley, J.-D. Chai, A. Dreuw, B. D. Dunietz, T. R. Furlani, S. R. Gwaltney, C.-P. Hsu, Y. Jung, J. Kong, D. S. Lambrecht, W. Liang, C. Ochsenfeld, V. A. Rassolov, L. V. Slipchenko, J. E. Subotnik, T. Van Voorhis, J. M. Herbert, A. I. Krylov, P. M. W. Gill, and M. Head-Gordon, "Advances in molecular quantum chemistry contained in the Q-Chem 4 program package," Mol. Phys. **113**, 184–215 (2015).
[83]R. Ditchfield, W. J. Hehre, and J. A. Pople, "Self-consistent molecular-orbital methods. IX. An extended Gaussian-type basis for molecular-orbital studies of organic molecules," J. Chem. Phys. **54**, 724–728 (1971).
[84]P. C. Hariharan and J. A. Pople, "The influence of polarization functions on molecular orbital hydrogenation energies," Theor. Chim. Acta **28**, 213–222 (1973).
[85]W. J. Hehre, R. Ditchfield, and J. A. Pople, "Self—Consistent molecular orbital methods. XII. Further extensions of Gaussian—Type basis sets for use in molecular orbital studies of organic molecules," J. Chem. Phys. **56**, 2257–2261 (1972).

[86]T. J. A. Wolf, R. H. Myhre, J. P. Cryan, S. Coriani, R. J. Squibb, A. Battistoni, N. Berrah, C. Bostedt, P. Bucksbaum, G. Coslovich, R. Feifel, K. J. Gaffney, J. Grilj, T. J. Martinez, S. Miyabe, S. P. Moeller, M. Mucke, A. Natan, R. Obaid, T. Osipov, O. Plekan, S. Wang, H. Koch, and M. Guhr, "Probing ultrafast pi pi*/n pi* internal conversion in organic chromophores via K-edge resonant absorption," Nat. Commun. **8**, 29 (2017).

[87]J. D. Coe and T. J. Martínez, "Competitive decay at two- and three-state conical intersections in excited-state intramolecular proton transfer," J. Am. Chem. Soc. **127**, 4560–4561 (2005).

[88]D. Jacquemin, V. Wathelet, E. A. Perpète, and C. Adamo, "Extensive TD-DFT benchmark: Singlet-excited states of organic molecules," J. Chem. Theory Comput. **5**, 2420–2435 (2009).

[89]T. Risthaus, A. Hansen, and S. Grimme, "Excited states using the simplified Tamm–Dancoff-approach for range-separated hybrid density functionals: Development and application," Phys. Chem. Chem. Phys. **16**, 14408–14419 (2014).

[90]S. Grimme and C. Bannwarth, "Ultra-fast computation of electronic spectra for large systems by tight-binding based simplified Tamm–Dancoff approximation (sTDA–xTB)," J. Chem. Phys. **145**, 054103 (2016).

[91]A. Hellweg, S. A. Grün, and C. Hättig, "Benchmarking the performance of spin-component scaled CC_2 in ground and electronically excited states," Phys. Chem. Chem. Phys. **10**, 4119–4127 (2008).

[92]F. Furche, R. Ahlrichs, C. Hättig, W. Klopper, M. Sierka, and F. Weigend, "Turbomole," Wiley Interdiscip. Rev.: Comput. Mol. Sci. **4**, 91–100 (2014).

[93]C. Song and T. J. Martínez, "Reduced scaling CASPT2 using supporting subspaces and tensor hyper-contraction," J. Chem. Phys. **149**, 044108 (2018).

[94]D. Asturiol, B. Lasorne, M. A. Robb, and L. Blancafort, "Photophysics of the π, π* and n, π* states of thymine: MS-CASPT2 minimum-energy paths and CASSCF on-the-fly dynamics," J. Phys. Chem. A **113**, 10211–10218 (2009).

[95]J. Segarra-Martí, A. Francés-Monerris, D. Roca-Sanjuán, and M. Merchán, "Assessment of the potential energy hypersurfaces in thymine within multiconfigurational theory: CASSCF vs. CASPT2," Molecules **21**, 1666 (2016).